Powder synthesis and spectroscopic properties of ytterbium-doped yttrium oxysulfide

Gang Yao (姚 罡), Liangbi Su (苏良碧), Xiaodong Xu (徐晓东), Lihe Zheng (郑丽和), and Jun Xu (徐 军)

Shanghai Institute of Optics and Fine Mechanics, Chinese Academy of Sciences, Shanghai 201800

Received August 14, 2007

Ytterbium-doped yttrium oxysulfide (Yb:Y_2O_2S) has been synthesized by solid-state reaction with sulfide flux. Diffuse reflection and emission spectra have been measured in order to determine the crystal field splitting of Yb^{3+} ion in the YOS lattice. According to the crystal-field levels probed in the spectra, the crystal field splitting of $^2F_{7/2}$ manifold of Yb^{3+} ion in YOS is 709 cm^{-1}, which is large enough for the quasi-three-level laser operation of Yb^{3+} ion. Emission peak position, width, full-width at half maximum (FWHM), and normalized intensity of Yb:YOS are fitted from its emission spectrum. For comparison, relevant data of 5.4 at.-% Yb:YAG is also provided.

OCIS codes: 160.3380, 160.4760, 300.2140.

As the development of high-efficiency laser diode in 1990s, the Yb^{3+} ion has been studied intensively as a competitor of Nd^{3+} in laser gain medium of all-solid-state laser system. The simple two electronic $^2F_{7/2}$ and $^2F_{5/2}$ manifolds of Yb^{3+} ions enables many advantages, such as high doping level, low excited states absorption and upconversion, leading to the miniaturization of devices[1]. Working in continuous wave (CW), passively Q-switched and passively locked modes, the Yb^{3+} ion has shown excellent laser properties in traditional laser crystals YAG[2−4]. It is also a very useful sensitizer for many laser active ions, such as Er^{3+}, Ho^{3+}, Pr^{3+}, Tm^{3+}, Nd^{3+}, and Cr^{4+} *et al.*.

It is well known that one main drawback of Yb lasers is that the fundamental and terminal energy levels of Yb^{3+} ions belong to the same manifold and so the gain medium will operate in quasi-three-lever scheme. In order to enhance laser performance of Yb^{3+} ions, the terminal state splitting should be as large as possible. This property is greatly affected by the crystal-field effect. For example, the $^2F_{7/2}$ manifold overall splitting is only 492 cm^{-1} in $CaWO_4$, whereas it reaches 1190 cm^{-1} in $Sr_5(PO_4)_3F$, which is one of the highest known values[5,6].

Lanthanide compounds have long been recognized for applications in various fields based on the electronic, magnetic, optical, and chemical characteristics arising from their 4f electrons[7]. Lanthanide oxysulfides received particular attention due to their high performance as fluorescence materials. They also have significant commercial applications in the field of radiation intensifying screens, X-ray-computed tomography, oxygen storage, and medical imaging radiation detectors[8−11].

Small crystal-field splitting of terminal level will be a great disadvantage for choosing La_2O_2S or Gd_2O_2S as Yb-doped host. In Ref. [12], Nd-doped lanthanum oxysulfide (Nd:La_2O_2S) was grown by the Bridgeman-Stockbarger technique. They concluded that active ions in La_2O_2S have larger absorption cross section, larger emission cross section, and lower lasing threshold than those in YAG[13]. However, the crystal-field splitting of $^4I_{9/2}$ manifold of the Nd^{3+} ion in La_2O_2S is 90 cm^{-1}, which is much smaller than that in YAG (860 cm^{-1})[13]. Most recently, Orlovskii *et al.* (calculated splitting of the $^4I_{9/2}$ manifold of Nd^{3+} is 257 cm^{-1} in Gd_2O_2S(GOS) [14] also gave support to the conclusion that lanthanide oxysulfide provides relatively weak crystal-field effect to dopant but owns strong absorption and emission.

But still, we want to take advantages of large absorption and emission cross section and find a lanthanide oxysulfide with large enough crystal-field effect. In this paper, we followed the empirical rule that same package of smaller ions with similar outer electron configuration could lead to stronger crystal field effect and chose to produce Yb:Y_2O_2S (Yb:YOS) by solid-state reaction. The spectroscopic properties of 5 at.-% Yb:YOS were measured and compared with 5.4 at.-%Yb:YAG.

The powder sample of Yb:Y_2O_2S was synthesized by flux assisted solid-state reaction method. The starting materials used were Yb_2O_3 (99.999%), Y_2O_3 (99.999%) and sulfur (99.9%). The molar ratio of Yb_2O_3/Y_2O_3 is 0.05. Considering the influence of different sulfide fluxes[15], we added Li_2CO_3 (99.9%, 0.5 in molar ratio to Y_2O_3) into the mixture of starting materials. Excess sulfur (2.5 in molar ratio of Y_2O_3) was contained to form positive sulfur vapor pressure. Then all four kinds of powder were thoroughly mixed and pressed to form a white-yellow precursor cake. The scheme of the stainless-steel crucible is given in Fig. 1. One Al_2O_3 crucible fitting for the size of the cake was used to prevent direct contact of sulfur and outer stainless steel. The space left for the Al_2O_3 crucible was also controlled to prevent too much sulfur loss from the reaction between oxygen and sulfur. In the next step, the whole system was put into muffle furnace, heated from room temperature to 1200 °C in 6 hours and kept at that temperature for 2 hours, then naturally cooled to room temperature. The directly obtained cake was then heated to 500 °C and kept at that temperature for 3 hours to remove left sulfur.

Powder sample for X-ray diffraction (XRD) and

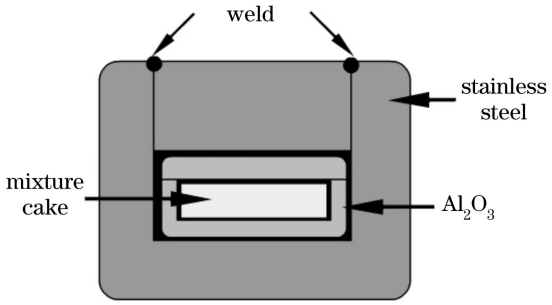

Fig. 1. Schematic setup of crucibles containing mixture cake.

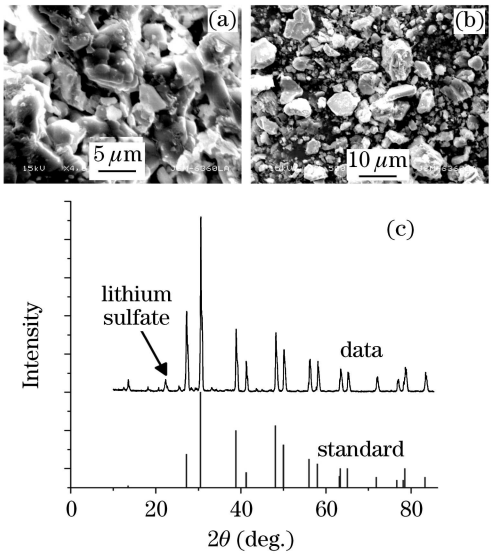

Fig. 2. SEM images of (a) surface of product cake, (b) ground powder, (c) XRD image of the powder.

spectroscopic measurements was prepared by thoroughly grinding the product cake without sulfur. The XRD data were collected using Rigaku D/MAX-2550-18 kW powder diffractometer with Cu Kα radiation at room temperature. Cake surface and powder morphology (Figs. 2(a) and (b)) without sulfur were investigated by JSM 6360A scanning electron microscope (SEM).

Diffuse reflection spectrum was measured by an integrating-sphere UV-VIS-NIR BWS003 spectrometer. Fluorescence spectrum was measured by TRIAX 550-type spectrophotometer made by Jobin-Yvon Company and the pumping source was a 940-nm laser. The samples were excited by laser diode (lambda = 940 nm) and its fluorescence lifetime was detected by an S1-photomultiplier. All data are obtained at room temperature and all wavelength sampling resolutions are smaller than 1 nm.

The reaction equation of producing lanthanide oxysulfide is

$$RE_2O_3 + \frac{3}{2}S \xleftrightarrow{1200\,^\circ C} RE_2O_2S + \frac{1}{2}SO_2. \quad (1)$$

Both the decomposing temperature of YOS and the balance temperature of reaction (1) is 1200 °C[16]. It is also near the creep temperature of stainless steel. In the reversible reaction (1), excess sulfur is needed to keep the reaction going to the positive direction. A proper time span of holding the crucibles at 1200 °C is also important. Our experiments showed that 2 hours is enough to complete the reaction under the condition that the raw material powders are mixed uniformly and compressed together tightly.

XRD peaks in Fig. 2(c) indicated the generation of well crystalline Yb:YOS phase (space group: P-3m). Single crystalline plate-like grains larger than 10 μm were observed before (Fig. 2(a)) and after (Fig. 2(b)) grinding. But no elongated and isometric grains appeared as mentioned in Ref. [16] and micro size tunnels spread through the cake, indicating that in a relatively loosen space, the YOS generated in situ will not automatically assemble into elongated grains, only if pressure is applied to force them to form a denser package with lower packaging energy.

Fluorescence spectrum of Yb:YOS is shown in Fig. 3. The ordinary emission peak of Yb^{3+} ions at $1040-1060$ nm seems to disappear in the YOS lattice. In order to precisely determine the $^2F_{7/2}$ manifold splitting of Yb^{3+} ions in YOS, the emission spectrum of this band ($1040-1060$ nm) was investigated and the weak emission peak located at 1051 nm of Yb:YOS was found out, which is shown in the inset of Fig. 3. The other three emission peaks are located at 981, 1013.5, and 1029 nm. The emission at 953 nm is related to thermal population and phonon-assisted emission.

After peak fitting of Fig. 3, fluorescence peak positions, full-width at half maximum (FWHM), and normalized intensities are listed in Table 1. The 1030-nm emission peak is dominant in Yb:YAG[17,18], while in YOS the strongest emission peak is at 981 nm. Also, there are two broadband emission peaks at 1013 nm and 953 nm. These broad emission bands may enable application of Yb:YOS in mode-locked ultra-short-pulse solid state lasers. Finally, the fluorescence intensity ratio of the emission peaks at 1013.5 nm and 981 nm reaches as high as 0.673, leading to the possibilities of tunable laser in Yb:YOS gain medium.

Figure 4 shows the diffuse reflection spectrum of 5 at.-% Yb:YOS. In the diffuse reflection spectrum, the valleys of the reflectance correspond to the peaks of absorption. Absorption peaks appear at 978, 952, and 923 nm. The main absorption is located at around 950 nm and the absorption at around 980 nm is much weaker, indicating that there is no strong self-absorption in Yb:YOS.

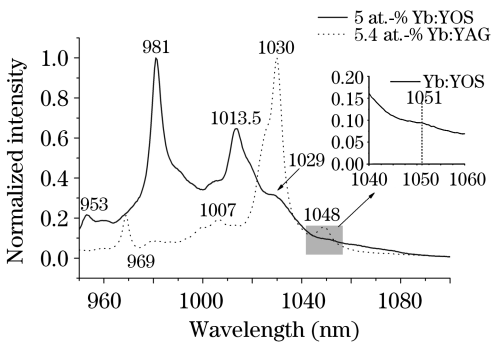

Fig. 3. Fluorescence spectra of 5 at.-% Yb:YOS powder and cake and 5.4 at.-% Yb:YAG[17] (inset: emission spectra of Yb:YOS from $1040-1060$ nm).

Table 1. Fluorescence Spectrum Peak Positions and Width of Yb:YOS and Yb:YAG

Material	5 at.-% Yb:YOS					5.4 at.-% Yb:YAG			
Position (nm)	953	981	1013.5	1029	1051	969	1007	1030	1048
FWHM (nm)	49.4	8.3	31.6	6.0	4.7	3.4	41.6	8.7	5.3
Normalized Intensity	18.2	100	67.3	7.7	9.4	34.7	15.3	100	11.2

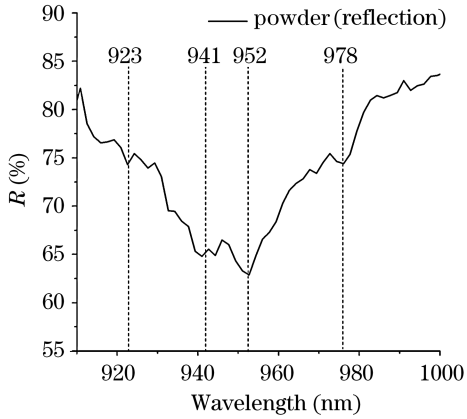

Fig. 4. Diffuse reflection spectrum of 5 at.-% Yb:YOS.

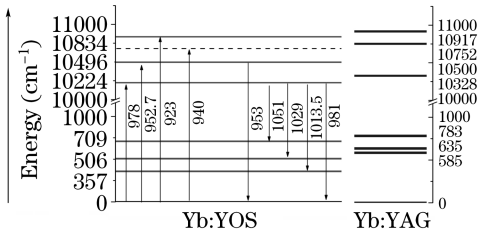

Fig. 5. Energy level schemes of 5 at.-% Yb:YOS and 5.4 at.-% Yb:YAG[1].

By adopting the data from the spectra, we drew the energy level scheme of Yb:YOS, as shown in Fig. 5. Calculating from the fluorescence and diffuse reflection spectrum, the terminal level splitting of Yb:YOS is 709 cm^{-1} (783 cm^{-1} in Yb:YAG) and the upper level splitting is 610 cm^{-1} (589 cm^{-1} in Yb:YAG). This means that the terminal level of Yb^{3+} splits to the same magnitude in YOS and YAG, and to a good enough extent for quasi-three-level laser operation. This phenomenon may result from the fact that the ionic radium of Y^{3+} is smaller than that of Gd^{3+}, La^{3+}. So, the rare-earth dopant in YOS is located in a more compact lattice than in GOS and LOS and experience stronger crystal-field effect resulted in larger crystal-field splitting. This also means that two manifolds of Yb^{3+} splits disproportionately in YOS and YAG and that it is unreliable to predict the splitting of all energy levels of ions (especially the ions with complex energy levels) merely from the point of host materials.

One may found red shift of emission and absorption peaks of the Yb^{3+} ion in YOS host, compared with Yb:YAG. This phenomenon can also be observed in Refs. [13] and [14] for Nd:LOS and Nd:GOS, compared with Nd:YAG. This phenomenon resulted from the nephelauxetic effect. In YAG lattice, the rare-earth ions are coordinated by oxygen ions, while in YOS lattice they are coordinated by oxygen and sulfur ions. The electronegtivity of sulfur (2.5) is smaller than that of oxygen (3.5). This leads to the decrease of ionicity and the increase of covalency of the bonds between rare-earth cations and coordinated anions, and the lowering of the energy gravity of rare-earth ions from that of YAG lattice to that of YOS lattice. So, the transitions between manifolds of energy levels appear to be red-shifted in the spectra.

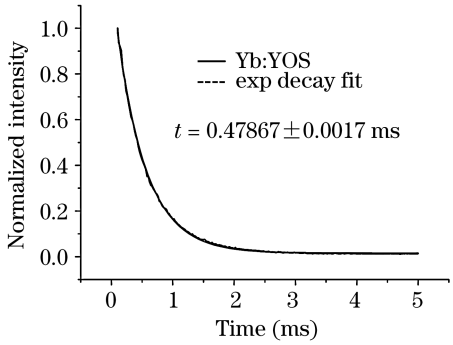

Fig. 6. Decay curve of 5 at.-% Yb:YOS fluorescence.

Upper-state lifetime of 5 at.-% Yb^{3+} in YOS was also tested. As shown in Fig. 6, the decay curve is well fitted by the first-order exponential-decay and the fitted lifetime $\tau = 0.478$ ms, which is not very long compared with some other Yb-doped hosts (eg., 15 at.-% Yb:YAP, $\tau = 1.50 - 1.54$ ms; 15 at.-% Yb:YAG, $\tau = 1.18 - 1.20$ ms[19]). This may be a disadvantage of the YOS host for CW laser output. However, dopant in lanthanide oxysulfide own greater absorption and emission cross section and lower lasing threshold than in YAG. Along with large terminal energy level splitting and low phonon energy (for YOS, it is 472.3 cm^{-1}[20]; for YAG it is 700 cm^{-1}[21]), Yb:YOS will be an excellent Yb-doped laser material. The efforts of crystal growth and ceramic sintering are already underway.

In conclusion, well crystalline 5 at.-% Yb:YOS powder was synthesized by solid-state reaction. Diffuse reflection and emission spectrum were tested to determine the crystal-field splitting of Yb^{3+} in YOS host. The splitting of $^2F_{5/2}$ manifold in YOS is 610 cm^{-1}, while that of $^2F_{7/2}$ manifold is 709 cm^{-1}, which are adequately large for quasi-three-level laser operation of Yb^{3+} ions. The emission spectrum of Yb:YOS is quite different from that of Yb:YAG, and there are two broad and strong wideband emission peaks in Yb:YOS. Newly discovered and already-known excellent properties clearly inform us that Yb:YOS will be a desirable laser material with new applications.

G. Yao's e-mail address is yourgun23shawn@gmail.com.

References

1. P.-H. Haumesser, R. Gaumé, B. Viana, E. Antic-Fidancev, and D. Vivien, J. Phys.: Condens. Matter. **13,** 5427 (2001).
2. D. J. Ripin, J. R. Ochoa, R. L. Aggarwal, and T. Y. Fan, Opt. Lett. **29,** 2154 (2004).
3. P. Yan, H. Wu, M. Gong, Q. Liu, C. Li, R. Z. Cui, and W. P. Jia, Opt. Laser Eng. **42,** 413 (2004).
4. F. Brunner, R. Paschotta, J. Aus der Au, G. J. Spühler, and F. Morier-Genoud, Opt. Lett. **26,** 379 (2001).
5. C. A. Morrison and P. Leavitt, *Handbook on the Physics and Chemistry of Rare Earths* (Amsterdam: Elsevier, 1982) p46.
6. J. B. Gruber, B. Zandi, and L. Merkle, J. Appl. Phys. **83,** 1009 (1998).
7. G. Liu, Bernard Jacquier (eds.) *Spectroscopic properties of Rare Earths in Optical Materials* (Tsinghua University Press, Beijing, 2005) p2.
8. S.-H. Yu, Z.-H. Han, J. Yang, H.-Q. Zhao, R.-Y. Yang, Y. Xie, Y.-T. Qian, and Y.-H. Zhang, Chem. Mater. **11,** 192 (1999).
9. M. Machida, K. Kawamura, K. Ito, and K. Ikeue, Chem. Mater. **17,** 1487 (2005).
10. D. Cavouras, I. Kandarakis, T. Maris, G. S. Panayiotakis, and C. D. Nomicos, Eur. J. Radio. **35,** 70 (2000).
11. L. D. da Vila, E. B. Stucchi, and M. R. Davolos, J. Mater. Chem. **7,** 2113 (1997).
12. L. E. Sobon, K. A. Wickersheim, R. A. Buchanan, and R. V. Alver, J. Appl. Phys. **42,** 3049 (1971).
13. R. V. Alver, R. A. Buchanan, K. A. Wickersheim, and E. A. C. Yates, J. Appl. Phys. **42,** 3043 (1971).
14. Yu. V. Orlovskii, T. T. Basiev, K. K. Pukhov, M. V. Polyachenkova, P. P. Fedorov, O. K. Alimov, E. I. Gorokhova, V. A. Demidenko, O. A. Khristich, and R. M. Zakalyukin, J. Lumin. **125,** 201 (2007).
15. P. Zhang, Z. Hong, Q. Huang, X. Fan, Z. Wang, G. Qian, and M. Wang, J. Chin. Ceram. Soci. **33,** 140 (2005).
16. G. V. Anan'eva, E. I. Gorokhova, L. N. Kinzhibalo, V. V. Kuprevich, T. I. Merkulyaeva, and O. A. Kristich, J. Opt. Technol. **66,** 404 (1999).
17. X. Xu, Z. Zhao, P. Song, G. Zhou, J. Xu, and P. Deng, J. Opt. Soc. Am. B. **21,** 543 (2004).
18. X. He, G. Zhao, X. Xu, X. Zeng, and J. Xu, Chin. Opt. Lett. **5,** 295 (2007).
19. X. Zeng, G. Zhao, X. Xu, H. Li, J. Xua, Z. Zhao, X. He, H. Pang, M. Jie, and C. Yan, J. Crystal Growth. **274,** 106 (2005).
20. M. Mikami, S. Nakamura, M. Itoh, K. Nakajima, and T. Shishido, J. Lumin. **102,** 7 (2003).
21. B. M. Walsh, J. M. McMahon, W. C. Edwards, N. P. Barnes, R. W. Equall, and R. L. Hutcheson, J. Opt. Soc. Am. B **19,** 2893 (2002).